2D filtered backprojection for fan-beam CT with independent rotations of the source and the detector

Simon Rit and Rolf Clackdoyle

***Abstract*—A cone-beam CT scanner has recently been developed for radiotherapy imaging where the source and the flat detector can rotate independently along concentric circular trajectories. This paper investigates the reconstruction of the central slice of this system. A new filtered-backprojection algorithm has been derived that only modifies the weighting schemes of the projections and the backprojections of the standard fan-beam algorithm. The accuracy of the algorithm is demonstrated on simulated projections of a numerical phantom with source and detector trajectories that image an offset field-of-view.**

I. Introduction

Cone-beam computed tomography (CT) scanners have been introduced in radiotherapy rooms to acquire three-dimensional (3D) CTs of patients prior to treatment and guide their delivery accordingly. Existing cone-beam CT scanners are generally fixed to the gantry of the linear accelerator with an x-ray source dedicated to imaging that is orthogonal to the treatment beam [1].

MedPhoton, a spin-off company of Paracelsus Medical University (Salzburg, Austria), is developing a new Patient Alignment system with an integrated x-ray Imaging Ring (PAIR, Figure 1). The system has been designed to provide greater flexibility in the positioning of the patients and to enable re-positioning of the patient based on 3D images acquired during radiotherapy. A robotic couch is mounted to the ceiling along which an imaging ring surrounding the patient table can translate in the cranio-caudal direction. The x-ray source and the flat panel detector are mounted on the ring and can rotate independently to acquire x-ray projections of any part of the patient with various incidences. The x-ray source is collimated with four motorized jaws that can dynamically adapt the dimension of the x-ray beam. The device allows, for example, the acquisition of x-ray projections for CT reconstruction with an offset field-of-view, i.e., a field-of-view that is not centered on the mechanical center-of-rotation.

By default, the source follows a conventional circular trajectory with respect to the patient and it is known that for this geometry, only the plane containing the source trajectory can be reconstructed exactly [2]. We limit our study to this plane. Two-dimensional (2D) filtered-backprojection (FBP) algorithms are known for the conventional situation where the flat detector is orthogonal to the line connecting the source to the center-of-rotation [3]. FBP formulas have also been derived for displaced centers-of-rotation [4] and for noncircular trajectories [5], [6] but these situations do not cover the geometry of PAIR's central slice.

S. Rit is with the Université de Lyon, CREATIS; CNRS UMR5220; Inserm U1044; INSA-Lyon; Université Lyon 1; Centre Léon Bérard, France (e-mail: simon.rit@creatis.insa-lyon.fr). R. Clackdoyle is with the laboratoire Hubert Curien, CNRS and Université Jean Monnet (UMR 5516), Saint Étienne, France. This work was partially supported by grants ANR-12-BS01-0018 (DROITE project) and ANR-13-IS03-0002-01 (DEXTER project) from the Agence Nationale de la Recherche (France).

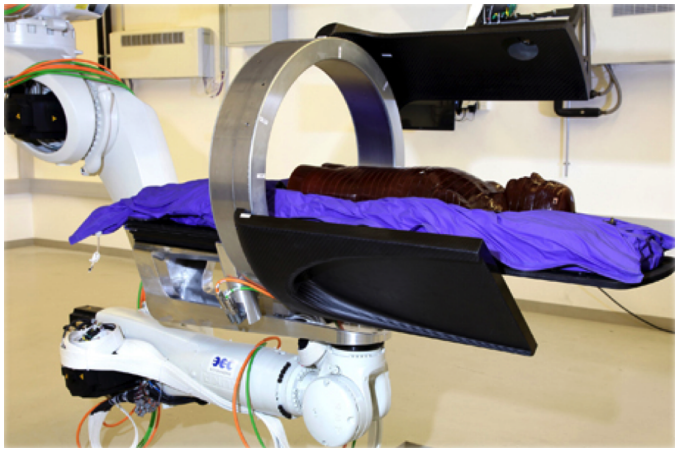

Fig. 1. Photography of a prototype of the Patient Alignment system with an Integrated x-ray imaging Ring (PAIR).

In this article, we derive a 2D FBP formula for circular trajectories with independent rotations of the source and the detector. The resulting algorithm is tested on simulated data in which the center of the field-of-view is not at the center-of-rotation.

II. Reconstruction algorithm

The geometry is described in Figure 2 with the origin at the center-of-rotation. The fan-beam source follows a circular trajectory parameterized by angle β and at fixed radius R from the center-of-rotation. The source motion is therefore given by $\boldsymbol{v} = (-R\sin\beta, R\cos\beta)$. The flat detector lies at fixed radius R_D from the center-of-rotation and is tilted at an angle α with respect to the usual position, which would be directly opposite the x-ray source. The detector and the source can rotate independently so the tilt angle may also vary with β, and α is understood to have a β dependence. The origin of the detector is at the point closest to the center-of-rotation as shown in Figure 2.

The aim is to reconstruct the unknown two-dimensional (2D) function $f(x, y)$ from the measured line integrals

$$g(\beta, u) = \int_0^\infty f(\boldsymbol{v} + t\boldsymbol{\gamma})\,\mathrm{d}t \qquad (1)$$

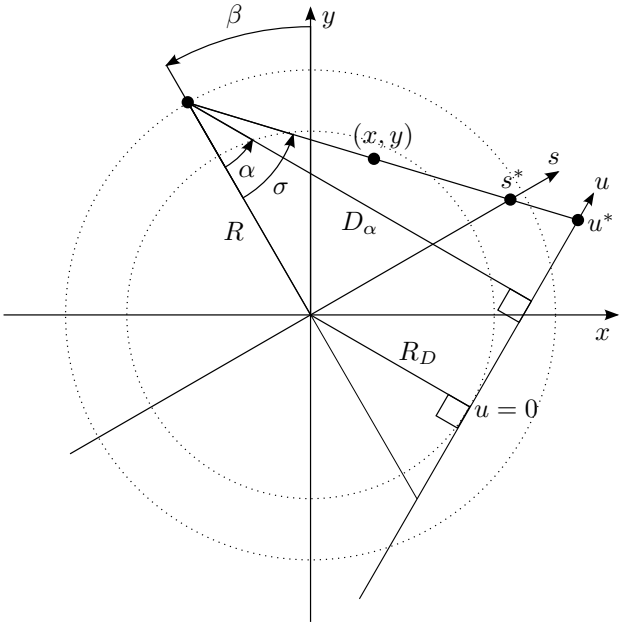

Fig. 2. Geometry of the central slice of the PAIR.

where $\boldsymbol{\gamma}$ is the unit vector pointing from source $\boldsymbol{v}$ to point u on the detector.

One method of reconstruction is to resample (or "rebin") the detector data to an equivalent virtual detector placed at the origin and oriented directly opposite the source to obtain projections $\overline{g}(\beta, s)$. This virtual detector corresponds to $\alpha = 0$ and $R_D = 0$, and is illustrated as the s-axis in Figure 2. From this geometry, the standard fan-beam reconstruction algorithm described as the *equispaced fan-beam* in [3] is

$$f(x,y) = \frac{1}{2}\int_0^{2\pi} b_\beta(x,y)\,\mathrm{d}\beta \tag{2}$$

with

$$b_\beta(x,y) = \frac{1}{U^2}\int_{-\infty}^{\infty} \cos\sigma\ \overline{g}(\beta,s)h(s^*-s)\,\mathrm{d}s. \tag{3}$$

$b_\beta(x,y)$ is the image obtained after filtering and backprojecting one projection $\overline{g}(\beta,.)$. The quantity $\cos\sigma = R/\sqrt{s^2+R^2}$ is the cosine of angle between the central ray and the ray intercepting point s on the detector. The function h is the usual ramp filter $h(s) = \int |\sigma| \exp(2\pi i s\sigma)\,\mathrm{d}\sigma$. The point s^* is where the point (x,y) projects onto the detector, as shown in Figure 2. The ratio $U = [R - (x,y)\cdot(-\sin\beta, cos\beta)]/R$ is the distance between the source and the line parallel to the detector at point (x,y), divided by the source to detector distance R.

Rebinning from measured g to virtual $\overline{g}$ has the usual problems of resolution loss which are compounded by the fact that even spacing in s does not correspond to even spacing in u. Therefore, we derive the mathematical expression of $b_\beta(x,y)$ using the measured projections g with a change of variable from s to u. The variables are linked by the following relation

$$u = \frac{s(R + R_D/\cos\alpha)}{R\cos\alpha + s\sin\alpha} - R_D\tan\alpha. \tag{4}$$

The change of variable invokes the Jacobian term

$$\mathrm{d}u = |J|\mathrm{d}s = \frac{R^2\cos\alpha + R_D R}{(R\cos\alpha + s\sin\alpha)^2}\,\mathrm{d}s. \tag{5}$$

The absolute value has been dropped because the condition $\cos\alpha > -R_D/R$ is always met assuming $\alpha \in (-\pi/2, \pi/2)$. We also find from Equation 4 that

$$u^* - u = \frac{R^2\cos\alpha + R_D R}{(R\cos\alpha + s^*\sin\alpha)(R\cos\alpha + s\sin\alpha)}(s^* - s). \tag{6}$$

Combining the well-known result $h(at) = \frac{1}{a^2}h(t)$ (see, e.g., [3]) with the last two equations, we obtain

$$h(s^*-s)\,\mathrm{d}s = \frac{R^2\cos\alpha + R_D R}{(R\cos\alpha + s^*\sin\alpha)^2}h(u^*-u)\,\mathrm{d}u \tag{7}$$

$$= \frac{R}{D_\alpha}\frac{D_\alpha^2}{(R\cos\alpha + s^*\sin\alpha)^2}h(u^*-u)\,\mathrm{d}u \tag{8}$$

where we have introduced the source to detector distance $D_\alpha = R_D + R\cos\alpha$. Note that D_α varies with α, unlike the source to center-of-rotation and the center-of-rotation to detector distances R and R_D which are fixed.

When u satisfies Equation 4, the measured and the rebinned projections are equal, i.e., $g(\beta,u) = \overline{g}(\beta,s)$, and the change of variables in Equation 3 gives

$$b_\beta(x,y) = \frac{1}{V^2}\int_{-\infty}^{\infty}\cos\sigma\frac{R}{D_\alpha}g(\beta,u)h(u^*-u)\,\mathrm{d}u \tag{9}$$

where

$$V = \frac{R\cos\alpha + s^*\sin\alpha}{D_\alpha}U \tag{10}$$

is to the real detector what U is to the virtual detector, i.e., the distance between the source and the line parallel to the detector at point (x,y) divided by the source to detector distance D_α. For more readability, we have not replaced the term $\cos\sigma$ but it may be expressed in terms of u by

$$\cos\sigma = \cos(\alpha + (\sigma - \alpha)) = \frac{D_\alpha\cos\alpha - (u - R\sin\alpha)\sin\alpha}{\sqrt{D_\alpha^2 + (u - R\sin\alpha)^2}}. \tag{11}$$

It is interesting to consider Equation 9 for the particular case of a virtual tilted detector passing through the center-of-rotation ($R_D = 0$). In this case, Equation 9 becomes

$$b_\beta(x,y) = \frac{1}{V^2}\int_{-\infty}^{\infty}\frac{\cos\sigma}{\cos\alpha}g(\beta,u)h(u^*-u)\,\mathrm{d}u \tag{12}$$

and we note that the reconstruction algorithm is the same as the reconstruction algorithm for the untilted case with three modifications: (1) the backprojection weighting $1/V^2$ is with respect to the tilted detector, (2) the $\cos\sigma$ weighting is with respect to the non-tilted detector and (3) there is an additional $1/\cos\alpha$ term in the weighting of the projections.

III. Experiments

The reconstruction algorithm has been validated on simulated projections. The fixed geometric parameters were chosen to be close to those of the PAIR: the radii of the source and the detector were $R = 700\,\mathrm{mm}$ and $R_D = 400\,\mathrm{mm}$ and the detector measured 1024 samples in the interval $u \in [-175.3, 233.9]\,\mathrm{mm}$. As in the PAIR, the center of the detector has been intentionnally shifted by $29.3\,\mathrm{mm}$ to enlarge the field-of-view when it is centered.

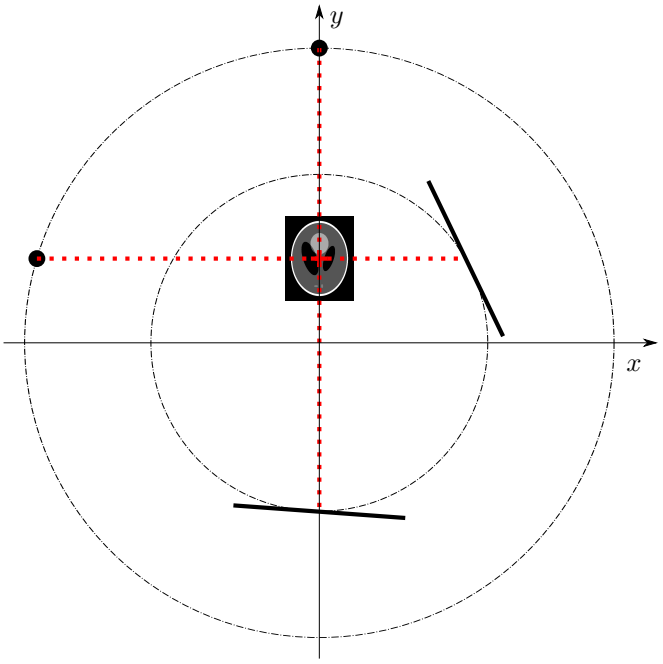

Fig. 3. Scale drawing of the experiment for the positions corresponding to projection #0 and projection #181. The phantom image is the reference slice in Figure 5. The red cross is the center of the offset field-of-view. The two red lines correspond to the source to center-of-detector lines of the two positions of the detector. The pair of angles (α, β) were about $(-4°, 0°)$ and $(42°, 73°)$ for projections #0 and #181, respectively. Corresponding vertical lines have been drawn in Figure 4. Note that the detector is not horizontal when the source to center-of-rotation line is vertical for projection #0 because the center of the detector that we align with this line is at $u = 29.3\,\mathrm{mm}$.

The angles α and β are two degrees of freedom of the scanner set by the user to acquire one projection $g(\beta, .)$. We centered the offset field-of-view on point $(0, 200)\,\mathrm{mm}$ of the y-axis (Figure 3). The source position β was set to enforce an equiangular spacing at the center of the offset field-of-view of the 720 projections. The variation of the speed of the source rotation (Figure 4) has been accounted for in the discretization of Equation 2 with a variable $\Delta\beta$-weight between projections. The tilt angle α was set to align the source, the center of the offset field-of-view and the center of the detector for every projection. Figure 4 illustrates the β and $\beta+\alpha$ values according to projection number where β is the angle of the source to center-of-rotation line with the y-axis and $\alpha + \beta$ is the angle of the detector with the x-axis (Figure 2). These curves would have been parallel lines if the offset field-of-view had been centered on the center-of-rotation but we varied the speed of the rotation of the source and the detector in order to focus on the chosen offset field-of-view.

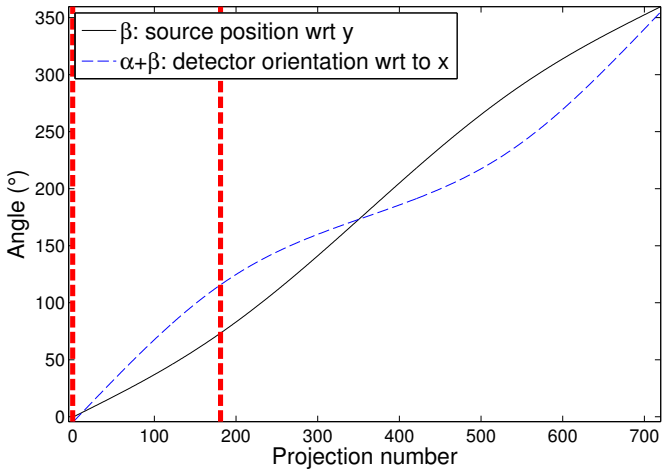

Fig. 4. Variations of β and $\alpha + \beta$ according to the projection number in the simulated projections of the phantom. Note that the source rotates more slowly (lower slope) when near the center of the offset field-of-view at the begin and the end of the scan. Similarly for the detector which is close to the offset field-of-view at the middle of the scan. The two vertical dashed lines correspond to the two positions that have been represented in Figure 3.

The phantom was slice $z = -0.25$ of the 3D version of the Shepp Logan phantom described in [3], centered on point $(0, 200)\,\mathrm{mm}$ and scaled to 69 by $92\,\mathrm{mm}$ to fill the offset field-of-view. The reconstruction lattice was also centered on this point and made of 400×500 pixels of $0.4 \times 0.4\,\mathrm{mm}^2$.

IV. Results

Several images of the phantom are shown in Figure 5: (1) the reference image illustrates the original phantom, (2) a naive modification of the existing equispaced FBP described in the following, and (3) the image obtained using the proposed fan-beam FBP algorithm. The naive modification of the existing equispaced FBP consisted in assuming that the source to center-of-rotation line was orthogonal to the detector during the weighting of projection images which comes down to weighting the projection by $\cos(\sigma - \alpha)$ instead of $\cos(\sigma)$ in Equation 9 while filtering and backprojecting the weighted projections in a similar manner. Images are displayed with two different gray scales, one to illustrate the large discrepancy between the naive reconstruction and the reference, and another narrow one to illustrate the accuracy of the new FBP algorithm.

Profiles along the lines drawn in Figure 5 are plotted in Figure 6. Accurate values have been reconstructed with small fluctuations ($\simeq 0.1\%$) around the expected values.

V. Discussion and Conclusions

A 2D FBP algorithm has been derived and validated for the reconstruction of the central slice of a cone-beam CT system, the PAIR, where the source and the detector can rotate independently. The new FBP algorithm is very similar to the conventional one [3]: only the weights of the projections and the backprojections need to be modified.

Other equispaced fan-beam geometries have been proposed but they did not cover this geometry. Gullberg *et al* derived

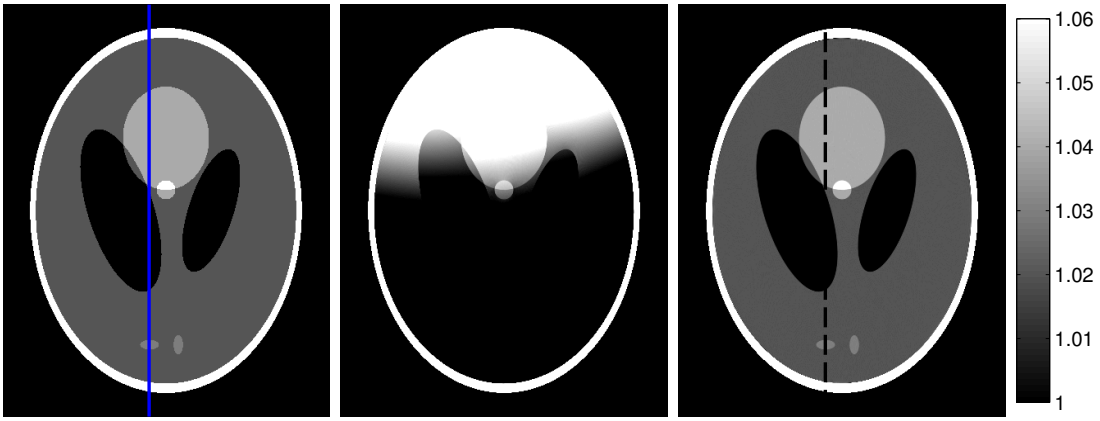

Fig. 5. Left: reference image of the phantom. Middle: naive modification of existing equispaced FBP. Right: new FBP algorithm.

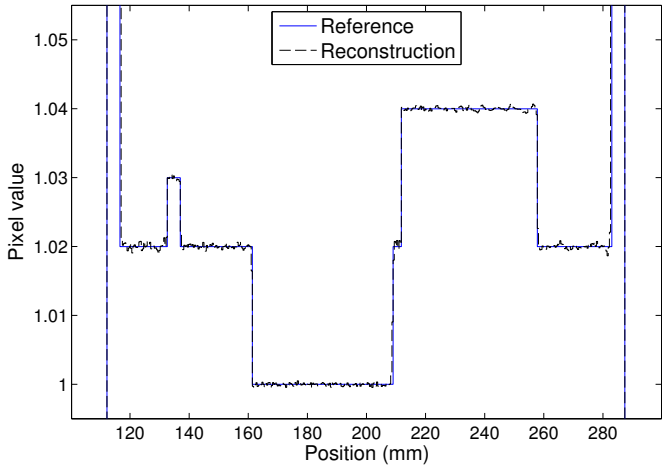

Fig. 6. Vertical profiles along the lines drawn on the reference and the reconstructed images of Figure 5.

a reconstruction formula for a fixed offset τ of the detector [4] which is covered by the new formula. Their formula may be obtained from Equation 9 by linking the parameterizations with $\tau = R \sin \alpha$. Other formulas are for non-circular source trajectories [5], [6].

Independent rotations of the source and the detector enable offset field-of-views. Offset field-of-views are essential in PAIR to image areas which could not be imaged otherwise due to the limited size of the detector. A side effect of moving the center of the offset field-of-view is the reduction of its maximum size with increasing distances between the center-of-rotation and the center of the offset field-of-view.

The formula is inaccurate if projections are truncated which is expected in many practical situations. One solution is to use a short scan with a source arc that is opposite the center of the offset field-of-view with respect to the center-of-rotation. Short scan acquisitions can be reconstructed with an appropriate weighting scheme as proposed for the conventional FBP algorithm [7], provided that the arc is greater than $\pi + 2\sigma_{\max}$ where $\sigma_{\max}$ is the maximum value taken by $|\sigma|$. An alternative is to use an appropriate weighting scheme that accounts for redundant acquisition lines to truncate projections on one side only [8]. If it is insufficient, the derivation of other algorithms for region-of-interest reconstruction [9] will be required.

Three-dimensional reconstruction is beyond the scope of this article. Exact reconstruction is only possible in the central plane but the FDK algorithm is commonly used [10]. Future work includes the derivation of a practical algorithm for the geometry of the PAIR.

References

[1] D.A. Jaffray, J.H. Siewerdsen, J.W. Wong, and A.A. Martinez, "Flat-panel cone-beam computed tomography for image-guided radiation therapy," *Int J Radiat Oncol Biol Phys*, vol. 53, no. 5, pp. 1337–1349, Aug 2002.

[2] H. Tuy, "An inversion formula for cone-beam reconstruction," *SIAM Journal of Applied Mathematics*, vol. 43, pp. 91–100, 1983.

[3] A.C. Kak and M. Slaney, *Principles of computerized tomographic imaging*. IEEE Press, 1988.

[4] G.T. Gullberg, C.R. Crawford, and B.M. Tsui, "Reconstruction algorithm for fan beam with a displaced center-of-rotation," *IEEE Trans Med Imaging*, vol. 5, no. 1, pp. 23–29, 1986.

[5] F.S. Weinstein, "Formation of images using fan-beam scanning and noncircular source motion," *JOSA*, vol. 70, no. 8, pp. 931–935, 1980.

[6] C.R. Crawford, G.T. Gullberg, and B.M. Tsui, "Reconstruction for fan beam with an angular-dependent displaced center-of-rotation," *Med Phys*, vol. 15, no. 1, pp. 67–71, 1988.

[7] D.L. Parker, "Optimal short scan convolution reconstruction for fanbeam CT," *Med Phys*, vol. 9, no. 2, pp. 254–257, 1982.

[8] P.S. Cho, A.D. Rudd, and R.H. Johnson, "Cone-beam CT from width-truncated projections," *Computerized Medical Imaging and Graphics*, vol. 20, no. 1, pp. 49–57, 1996.

[9] R. Clackdoyle and M. Defrise, "Tomographic reconstruction in the 21st century," *IEEE Signal Process. Mag.*, vol. 27, no. 4, pp. 60–80, 2010.

[10] L.A. Feldkamp, L.C. Davis, and J.W. Kress, "Practical cone-beam algorithm," *J Opt Soc Am A*, vol. 1, no. 6, pp. 612–619, 1984.